Modelling of stone columns reinforces railway embankments: Coupled DEM-FDM analysis

Trung Ngo, Ph.D, M.ASCE[1] , Buddhima Indraratna, Ph.D, FASCE[2] and Cholachat Rujikiatkamjorn, Ph.D, M.ASCE[3]

[1]Senior lecturer, Transport Research Centre, School of Civil and Environmental Engineering, University of Technology Sydney, Ultimo, Australia (Corresponding author). ORCID: https://orcid.org/0000-0002-9676-3728. Email: Trung.Ngo@uts.edu.au
[2]Distinguished Professor of Civil Engineering and Director of Transport Research Centre, University of Technology Sydney, Ultimo, Australia. Email: buddhima.indraratna@uts.edu.au
[3]Professor, Transport Research Centre, School of Civil and Environmental Engineering, University of Technology Sydney, Ultimo, Australia.
Email: cholachat.rujikiatkamjorn@uts.edu.au

ABSTRACT

Stone columns have been increasingly adopted as an environmentally friendly and cost-effective method for stabilizing and reinforcing soft grounds embankments. This paper presents a coupled modelling using the discrete element method and continuum modeling approach to study the load-deformation responses of stone columns. In the coupled discrete-continuum model, a soft soil domain under an embankment is simulated by the continuum method (i.e., finite difference method -FDM), while a stone column is simulated by the discrete element method (DEM). A series of interface elements are introduced to facilitate the force-displacement transmission of both domains. The DEM transfers moment and contact forces to the FDM, and then the FDM moves displacements back to the DEM. The model is calibrated and further validated by experimental data. Contact force distributions and shear stress contours developed in the stone column and surrounding clay are captured to provide a better understanding of the load-deformation responses of the stone column from a micromechanical perspective.

INTRODUCTION

Among various methods that are commonly adopted in ground improvement for road and rail track embankments that can allow some settlements, stone columns have often been considered as a satisfactory solution and thus are increasingly used in practice (Black *et al.* 2011; Castro and Sagaseta 2011; Elshazly *et al.* 2007; Indraratna et al. 2018). The stone column has been used worldwide to increase the bearing capacity of soils and reduce long-term settlements of superstructures constructed on them. The main advantages of the stone column are: (1) to create a composite mass and to transfer loads through end bearing and frictional side resistance; and (2) to eliminate the total and differential settlements; (3) to reduce liquefaction potentials of soils (Mohamedzein and H. 2011; Bouassida *et al.* 1995; Deb 2010; Chai *et al.* 2010; Zhou et al. 2021;

Siahaan *et al.* 2011), among others. Guetif et al. (2007) reported that the stone columns act as reinforcement, possessing greater strength and stiffness compared to surrounding soils, but they also increase the dissipation of excess pore water pressure that is caused by surcharge loading and due to reducing drainage paths. Load-deformation responses of stone columns reinforce soft soils, and track embankments have been the subject of an extensive number of experimental and numerical studies during the past decades (Almgir *et al.* 1996; Indraratna *et al.* 2017; Chai *et al.* 2010; Sivakumar *et al.* 2011; Basack et al. 2022), among others. Most of these studies assumed the unit cell concept to be valid, where it represents a tributary area for each individual column (Lee *et al.* 2004; Castro and Sagaseta 2011; Indraratna *et al.* 2015), among others.

It is noted that a continuum-based modelling approach has provided valuable insights into the lateral displacements (bulging), vertical settlements, stress and strain-rate dependent responses of stone columns at the macroscopic scale. However, owing to the discrete nature of stone columns, which are comprised of granular materials (e.g., latile basalt, crushed rock or gravel), which could not be accurately captured by the conventional continuum approach (Song et al., 2019; Ngo and Indraratna 2020). The surrounding soil and a stone column interact with each other during the application of loading, and hence it remains a challenging task to incorporate them into a coupled numerical model. It is noted that there have still been limited studies on the interaction between a stone column and soft soils whereby the load is transmitted from the stone columns to the soils from a micromechanics perspective. This paper attempts to couple the discrete element method (DEM) and finite difference method (FDM) to examine the load-deformation responses of soils reinforced by a single stone column adopting the unit cell concept. The salient aim is to take advantage of each computational modeling method to minimize the computational resources needed. Details of the coupled DEM-FDM model were discussed earlier by Indraratna *et al.* (2015). Principally, coupling between the DEM and FDM is achieved by taking the contact forces with wall facets and determining an equivalent force at the nodes using shape functions. The predicted load-deformation behavior obtained from the numerical simulations was compared with those published in the literature to verify the reliability and accuracy of the proposed coupling model.

COUPLED DISCRETE-CONTINUUM MODELING APPROACH

A schematic figure of the coupled discrete-continuum model adopted to investigate the load-deformation response of stone column reinforced soils is depicted in Figure 1. The model dimensions are based on the model test carried out by Sivakumar et al. (2011). The model tests were conducted on soft clay (400 mm high, 300 mm in diameter) subjected to static loading. As a scaled model was selected, a relatively low area of replacement ratio (1.8% to 4%) was simulated in the numerical model to reduce computational effort. A stone column that is comprised of discrete particles was modelled by the DEM, using PFC2D software (Itasca 2014). In contrast, surrounding clay soils were simulated by the FDM, using FLAC software (Itasca 2014). The DEM transfers moment and forces to the FDM, and then the FDM updates wall displacement (i.e.,

velocity) back to the DEM model to execute a coupling simulation. It is noted that PFC2D and FLAC share similar geometrical boundaries where they are interfaced. Elements in the FLAC zone that are close to the interface had small sizes within a tolerable range for small discrete particles. Initially, a number of walls were created in DEM, in which each wall was used as an element in the FLAC zone. Subjected to external loads, the continuum meshes (in FLAC zones) deform, and nodal displacements are transferred back to the DEM, so that the walls move in exactly the same as the boundary elements of the FLAC. Due to particles interacting with the walls, the resulting wall forces are transferred to FLAC as applied nodal forces.
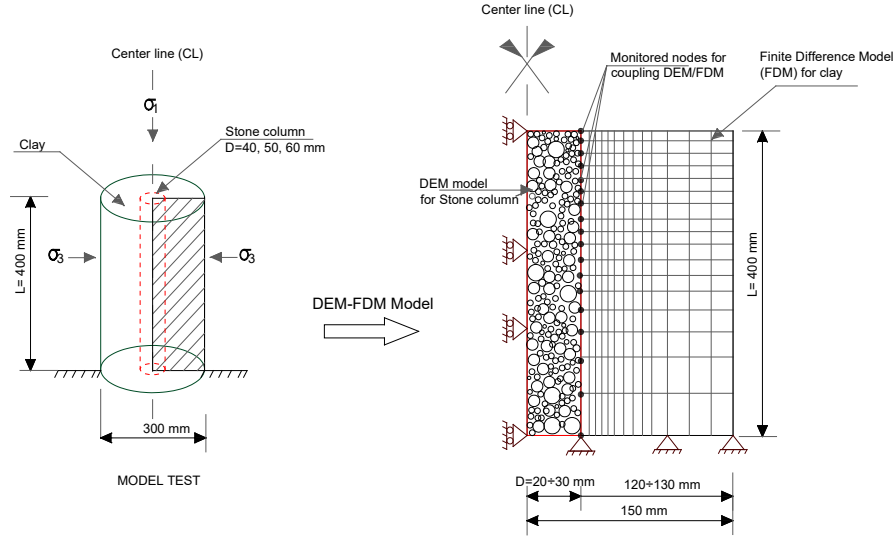

Figure 1. Schematic diagram of coupling DEM-FDM to model stone column (Source: Indraratna *et al*. 2015 – with permission from Elsevier)

Framework for coupling between the discrete and continuum domain
Contact forces at the interface, $F_i^{[C]}$, can be described by a normal force $F_{ni}^{[C]}$ and a shear force $F_{si}^{[C]}$ as illustrated in Figure 2a, as given by:

$$F_i^{[C]} = F_{ni}^{[C]} + F_{si}^{[C]} \tag{1}$$

The normal contact force is calculated as:

$$F_{ni}^{[C]} = k_n U^n n_i \tag{2}$$

where, k_n: normal contact stiffness, U^n: normal displacement, n_i: unit vector.

At any time, the shear contact force is computed by the increment form of the shear force, which can be computed by the relative shear displacement, knowing the shear stiffness (k_s).

The relative contact velocity at the interface, V_i is calculated by:

$$V_i = \dot{x}_{i,E}^{[C]} - \dot{x}_{i,B}^{[C]} \tag{3}$$

where, $\dot{x}_{i,E}^{[C]}$ and $\dot{x}_{i,B}^{[C]}$ are velocities of continuum elements and particles at their interface. The component $\dot{x}_{i,B}^{[C]}$ is determined as follows:

$$\dot{x}_{i,B}^{[C]} = \dot{x}_{i,B}^{[C]} + e_{ijk}\omega_3^{[B]}\left(x_i^{[C]} - x_i^{[B]}\right) \tag{4}$$

where, $\omega_3^{[B]}$ is the rotational velocity and e_{ijk} is the permutation symbol.

The velocities of the FLAC elements can then be calculated by interpolating into the nodal velocities, are described as:

$$\dot{x}_{i,E}^{[C]} = \sum N_j \dot{x}_{i,E}^j \tag{5}$$

where, $\dot{x}_{i,E}^j$: the nodal velocity of the continuum element j, and N_j is the shape function, as given by:

$$N_j = \frac{L - \sqrt{(x-x_i)^2 + (y-y_i)^2}}{L} \qquad (i = 1,2) \tag{6}$$

$$L = \sqrt{(x_1 - x_2)^2 + (y_1 - y_2)^2} \tag{7}$$

The increment of contact displacement per time step (Δt) at the interface, is determined by:

$$\Delta x_i^{[C]} = V_i \Delta t = \Delta x_{ni}^{[C]} + \Delta x_{si}^{[C]} \tag{8}$$

$$\Delta x_{ni}^{[C]} = \Delta x_i^{[C]} n_i \tag{9}$$

thus, $\Delta x_{si}^{[C]} = \Delta x_i^{[C]} - \Delta x_{ni}^{[C]} = \Delta x_i^{[C]} - \Delta x_i^{[C]} n_i \tag{10}$

where, $\Delta x_{ni}^{[C]}$ and $\Delta x_{si}^{[C]}$: normal and tangential vectors of the increment of contact displacement.

The increment of corresponding contact shear force per time step (Δt) is calculated as:

$$\Delta F_{si}^{[C]} = -k_s \Delta x_{si}^{[C]} \tag{11}$$

The new component of contact shear force is computed by the superposition of the shear force and the contact shear force increment, as given:

$$F_{si}^{[C]} \leftarrow \Delta F_{si}^{[C]} + F_{si}^{[C]} \leq \mu \Delta F_{ni}^{[C]} \tag{12}$$

where, μ: the coefficient of friction.

The resultant forces and moments acting on the contacted particle are determined by:

$$F_i^{[B]} \leftarrow F_i^{[B]} - F_i^{[C]} \tag{13}$$

$$M_i^{[B]} \leftarrow M_i^{[B]} - e_{ijk} \left(x_j^{[C]} - x_j^{[B]} \right) F_i^{[C]} \tag{14}$$

where, $F_i^{[B]}$ and $M_i^{[B]}$ are the superposition of the contact forces and the moments on the contacted particle; $x_j^{[C]}$ and $x_j^{[B]}$ are the contact point coordinates and center coordinates of the contacted particle (Figure 2a).

It is noted that interface elements only consider forces and moments applied at their nodes (F_{XA}, F_{YA}, F_{XB}, F_{YB}). Hence, forces and moments from a discrete particle (F_X, F_Y and M) need to be moved to the nodes of a continuum element, as described in Figure 2b. Taking the force equilibrium in the X and Y directions, the following equations can be derived:

Equilibrium forces in the horizontal direction: $\quad F_X = F_{X_A} + F_{X_B} \tag{15}$

Equilibrium force in the vertical direction: $\quad F_Y = F_{Y_A} + F_{Y_B} \tag{16}$

Equilibrium of moments at the centroid of an element can be described as:

$$M = F_{Y_A}(X_A - X_C) + F_{Y_B}(X_B - X_C) - F_{X_A}(Y_A - Y_C) - F_{X_B}(Y_B - Y_C) \tag{17}$$

Equations 15 and 16 can be described alternatively as:

$$F_X = F_{X_A} + F_{X_B} = \Omega \times F_X + (1 - \Omega) \times F_X \tag{18}$$

$$F_Y = F_{Y_A} + F_{Y_B} = \Omega \times F_Y + (1 - \Omega) \times F_Y \tag{19}$$

in which, the parameter Ω is given as follows:

$$F_{X_A} = \Omega \times F_X \quad \text{and} \quad F_{Y_A} = \Omega \times F_Y \tag{20}$$

$$F_{X_B} = (1 - \Omega) \times F_X \quad \text{and} \quad F_{Y_B} = (1 - \Omega) \times F_Y \tag{21}$$

Substituting Eq. 23, 24 in to Eq.20, results in :

$$M = \Omega \times F_Y \times (X_A - X_C) + (1 - \Omega) \times F_Y \times (X_B - X_C) - \Omega \times F_X \times (Y_A - Y_C) - (1 - \Omega) \times F_X \times (Y_B - Y_C) \tag{22}$$

$$\Omega = \frac{M - F_Y \times (X_B - X_C) + F_X \times (Y_B - Y_C)}{F_Y \times (X_A - X_B) - F_X \times (Y_A - Y_B)} \tag{23}$$

Eq. 23 can be used with Eq. 20 and 21 to exchange forces and moments from the DEM to the FDM model. The authors developed subroutines written in the FISH programing language to implement all the Equations above to execute a fully coupled DEM-FDM analysis.
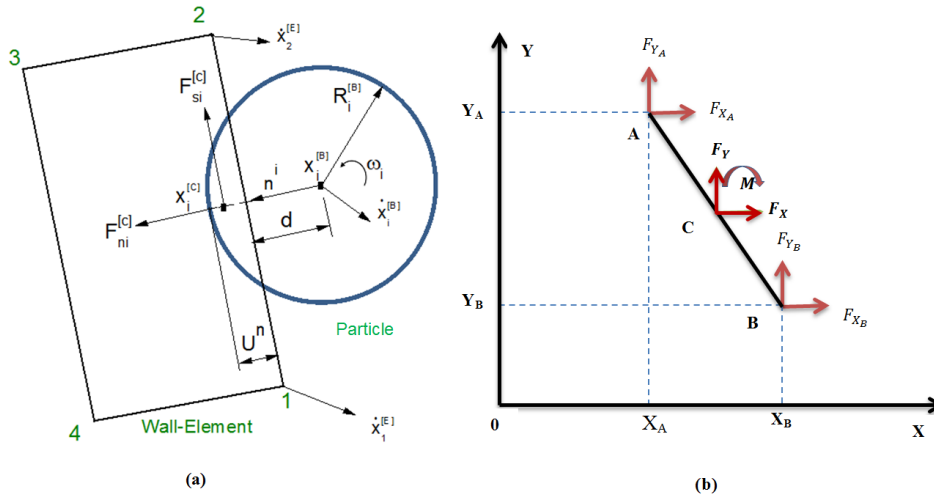

(a)   (b)

Figure 2. (a) notation used for coupling between a particle and a continuum element; (b) diagram of exchanging forces and moment to nodal forces (Indraratna et al. 2015)

Micromechanical parameters adopted for the numerical analysis

Crush rock aggregates were used to simulate stone columns, having relatively uniform grading with particle sizes between 2.5 and 3 mm. The angular shaped aggregates of the stone column were simulated using clusters of circularly-bonded particles. Micro-mechanical parameters to model the aggregates were chosen based on calibration with laboratory data presented by Sivakuma et al. (2011) and described in Table 1. Initially, micro-mechanical parameters (k_n, k_s, μ) adopted for DEM model of a 20 mm-diameter stone column was assumed. The coupled DEM–FDM was then performed, and a set of micro-mechanical parameters was selected until a

reasonable agreement between the prediction and laboratory data was achieved. Three stone columns with varying diameters of D=40, 50, and 60 mm were modelled in DEM (scaled model). The unit cell concept was applied to simulate surrounding soft soils under axisymmetric conditions. The soft clay was simulated in FLAC using the conventional Mohr-Coulomb's constitutive model. Surrounding soils were modelled as un-drained, and a total stress analysis was considered, given the scope of the current coupled DEM-FDM analysis. The input parameters used to model soft soil in the FDM model, including Modulus of elasticity, E = 4000 (kPa), Poison ratio, ν=0.4, undrained shear strength, c_u =20 (kPa), and density, γ =15 (kN/m^3).

Table 1. Micromechanical parameters used in DEM

Micro-mechanical parameters	Values
Contact normal stiffness, k_n (N/m)	0.42×10^7
Contact shear stiffness, k_s (N/m)	0.21×10^7
Inter-particle coefficient of friction μ	0.75
Contact normal stiffness of wall-particle, $k_{n\text{-}wall}$ (N/m)	1×10^7
Shear stiffness of wall-particle, $k_{s\text{-}wall}$ (N/m)	1×10^7
Particle density (kg/m^3)	18.5
Particle sizes (mm)	1.5-3

Validation of coupled DEM-FDM model

The applied vertical stress-settlements of a stone column carried out by Sivakumar *et al.* (2011) were adopted here to calibrate the introduced DEM-FDM model. Loading was applied to the top of the column and increased until maximum settlement was achieved. Figure 3 presents the comparison of vertical stresses and settlements predicted by the model with those measured in the laboratory for stone columns having D=40, 50, and 60 mm. It is seen that, in general, the predicted stress-settlement curves reasonably match well with experimental data, albeit the coupling analysis showed some discrepancy for the settlement of 4–10mm. Although the exact causes for these differences is not justified and will need to be subjected to further analysis, they are probably related to uncertainties in the model tests and assumptions made for the numerical simulations where the current analysis did not consider the correct shape of the particles.
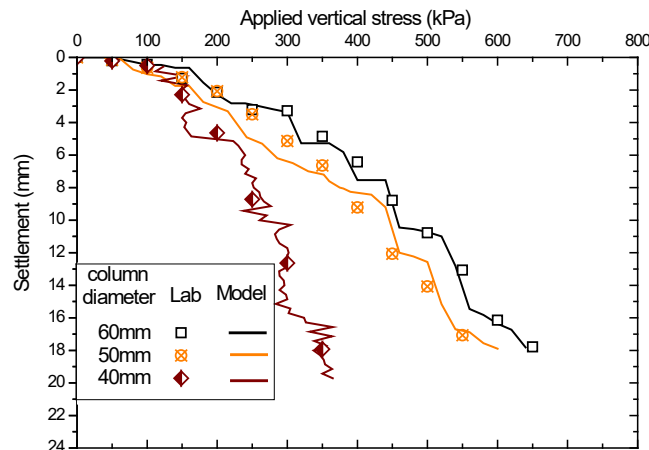
Figure 3. Comparisons of applied vertical stress-settlement responses between the coupled DEM-FDM analysis and experimental data (Source: Indraratna et al. 2015)

Figure 4 presents the predicted lateral displacements of stone columns with depth. It is seen that all three simulated stone columns deform and result in the bulging into surrounding soils that occurs at the portion close to the top of the columns. With an increase in the diameter of the column, the lateral displacements of the stone column significantly decrease, as expected. The bulging zone developed to about 100 mm from the stone columns' surface (ground level) and then started to decline with depth. This observation could be related to bulging that results in increased lateral confinement in the upper part of the column and induces changes in the orientations of contact forces within the granular media.
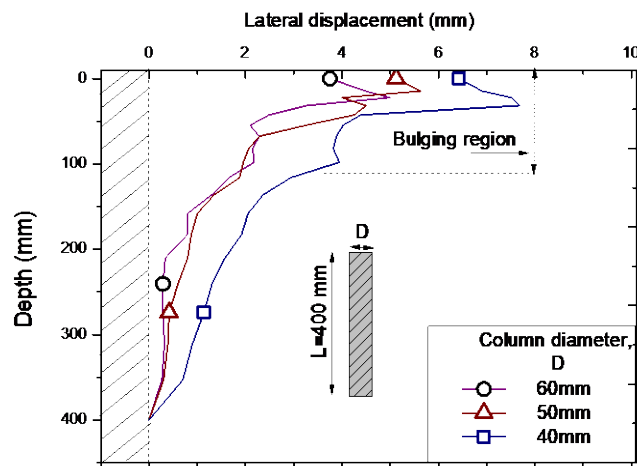

Figure 4. Predicted horizontal displacements of stone column (Indraratna et al. 2015)

The comparison of stress distribution at three locations in a stone column (PC1, PC2, and PC4) obtained from the coupled model and those presented by Sivakumar et al. (2011) is presented in Figure 5. Here, the predicted vertical stresses at three different locations agree reasonably well with those measured in the laboratory. As expected, the stresses decrease with depth, mainly because bulging occurs close to the stone column's ground surface, assisting the load transfer mechanism between stone columns and surrounding soils. Applied load onto the column was transferred to the soils as the lateral stress increased, causing bulging and mobilizing friction at the interface between them. Not surprisingly, there are some differences in the distributions of vertical stress with depth between the numerical predictions and the experimental data. Apart from these disparities, the proposed coupled DEM-FDM model could capture applied stress-settlement responses of stone columns.

Predicted contact force distributions
Deformation of stone columns will result in induced changes in the orientation of contact force within its structure. The micromechanical analysis discussed herein concentrates on the evolutions of contact force chains within the stone column assembly at different stages of settlement. Figure

6 shows the interparticle contact force chains for a stone column (40mm-diameter) at varying settlements *S*, varying from 0 to 15 mm. Contact forces among particles were plotted as lines whose thickness is proportional to the intensity of the force. It is predicted that the maximum contact forces and the total number of contact forces increase with an increase of settlements. This could be attributed to the compression of a stone column to sustain the applied load and bulging into the surrounding soils.
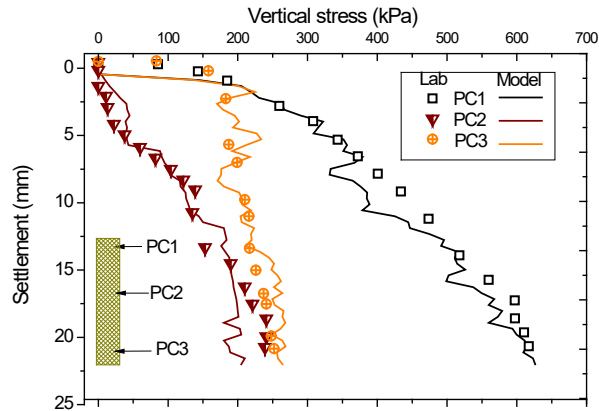

Figure 5. Comparisons of vertical stress distribution at different depths of stone column, D=50mm (Source: Indraratna *et al.* 2015– with permission from Elsevier)
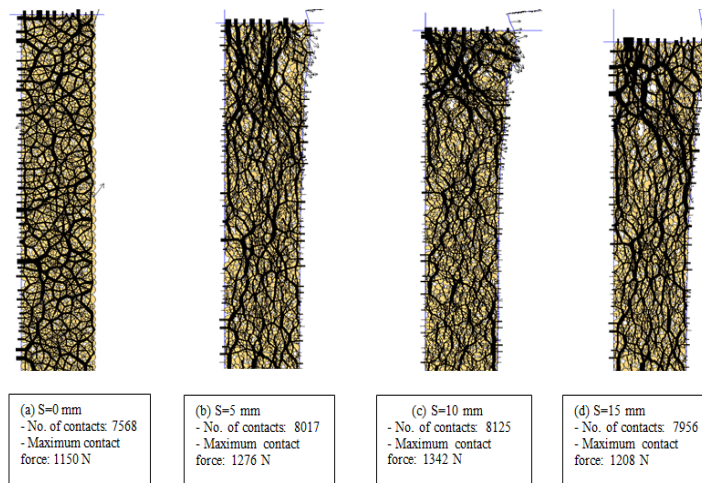

(a) S=0 mm	(b) S=5 mm	(c) S=10 mm	(d) S=15 mm
- No. of contacts: 7568	- No. of contacts: 8017	- No. of contacts: 8125	- No. of contacts: 7956
- Maximum contact force: 1150 N	- Maximum contact force: 1276 N	- Maximum contact force: 1342 N	- Maximum contact force: 1208 N

Figure 6. Contact force distributions of a stone column at different settlements: (a) *S*=0 mm; (b) *S*=5 mm; (c) *S*=10 mm; and (d) *S*=15 mm (Source: Indraratna et al. 2015)

Shear stress developed in the surrounding soils

Figure 7 shows shear stress contours induced in the surrounding soils stabilized by a stone column (40mm-diameter) predicted at *S*=5mm and 15mm. It is observed that the shear stress developed non-uniformly in the surrounding soils, and its magnitude depends upon vertical or lateral deformations (levels of bulging). In fact, the shear stress contour tends to concentrate in the upper part of the stone column (close to the ground surface), where the bulging occurs. The maximum

shear stress occurs within the bulging region, and their magnitudes increase with an increase in settlement, as measured in the laboratory. The maximum shear stress at the settlement of 15 mm was remarkably greater than those at the settlement of 5 mm (e.g., shear stress =16 kPa compared to 8 kPa, respectively). This could be attributed to the increased horizontal bulging of the stone column, where the bulging of the stone column is prevented by mobilizing frictional stresses at the interface with the surrounding soils.
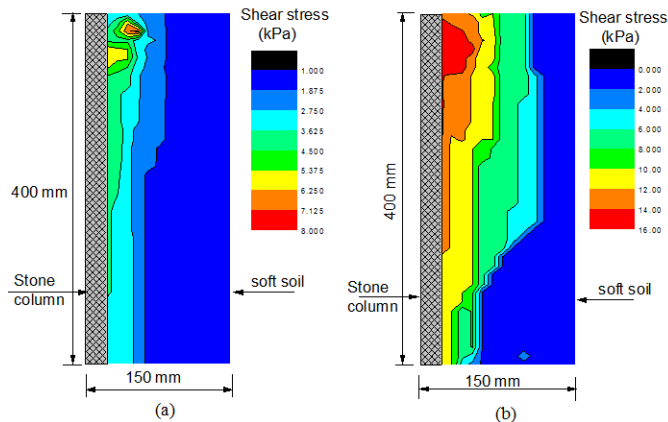

Figure 7. Shear stress contour: (a) *S*=5 mm, and (b) *S*=15 mm (Indraratna *et al*. 2015)

CONCLUSIONS

This paper presented a coupled discrete and finite-difference model to study load-deformation responses of a stone column stabilized subgrade soils for road and rail embankments. Coupling between the DEM and FDM was facilitated through a number of interface elements created at the discrete and continuum media boundary. The predicted results of stress-settlement behavior were reasonably comparable with the measured data (scaled model), showing that the coupled DEM-FDM model introduced in this study could be adopted to predict the load-displacement responses of stone columns stabilize soft soils. Contact force distributions and contours shear stresses mobilized in a stone column, and surrounding soils were analyzed to better understand the potential bulging phenomenon of the column under loading. The maximum contact forces and the total number of contact were found to increase with the increased settlement, and this could be attributed to the compression of a stone column under the external load and the associated bulging of the upper part of the column into the surrounding soils.

ACKNOWLEDGEMENTS

REFERENCES

Almgir, M., Miura., Poorooshasb, and Madhav, M. R. (1996). "*Deformation analysis of soft ground reinforced by columnar inclusions*". Computers and Geotechnics. 18(4): 267-290.

Black, J. A., Sivakumar, V. , and Bell, A. (2011). "*The settlement performance of stone column foundations*". Géotechnique. 6(11): 909-922.

Bouassida, M., Buhan, P. D. , and Dormieux, L. (1995). "*Bearing capacity of a foundation resting on a soil reinforced by a group of columns*". Geotechnique. 45(1): 25-34.

Basack, S., Nimbalkar, S., Karakouzian, M., Bharadwaj, S., Xie, Z. and Krause, N., 2022. *Field Installation Effects of Stone Columns on Load Settlement Characteristics of Reinforced Soft Ground*. International Journal of Geomechanics, 22(4), p.04022004.

Castro, J. , and Sagaseta, C. (2011). "*Deformation and consolidation around encased stone columns*". Geotextiles and Geomembranes. 29(3): 268-276.

Chai, J. C., Miura, N., kirekawa, T. , and Hino, T. (2010). "*Settlement prediction for soft ground improved by columns*". Ground Improvement. 163(2): 109-119.

Deb, K. (2010). "*A mathematical model to study the soil arching effect in stone column-supported embankment… soil*". Applied Mathematical Modelling. 34(12): 3871-3883.

Elshazly, H., Hafez, D. , and Mossaad, M. (2007). "*Settlement of circular foundations on stonecolumn- reinforced grounds*". Ground Improvement. 11(3): 163-170.

Guetif, Z., Bouassida, M. , and Debats, J. M. (2007). "*Improved soft clay characteristics due to stone column installation*". Computers and Geotechnics. 34(2): 104-111.

Indraratna, B., Ngo, N. T., Rujikiatkamjorn, C. , and Sloan, S. W. (2015). *"Coupled discrete element–finite difference method for analyzing the load-deformation behaviour of a single stone column in soft soil*". Computers and Geotechnics. 63: 267-278.

Indraratna, B., Ngo, N.T. and Rujikiatkamjorn, C., 2017. *Improved performance of ballasted rail tracks using plastics and rubber inclusions*. Procedia engineering, 189, pp.207-214.

Indraratna, B., Ferreira, F.B., Qi, Y. and Ngo, T.N., 2018. *Application of geoinclusions for sustainable rail infrastructure under increased axle loads and higher speeds*. Innovative Infrastructure Solutions, 3(1), pp.1-21.

Itasca, 2014. *Particle Flow Code*, Version. 5.0. Itasca Consulting Group. Minneapolis, MN.

Lee, F. H., Juneja, A. , and Tan, T. S. (2004). "*Stress and pore pressure changes due to sand compaction pile installation in soft clay*". Geotechnique. 54(1): 1-16.

Mohamedzein, Y. E. A. , and H., A.-S. I. (2011). "*Performance of an embankment supported on soft soil reinforced by stone columns*". Ground Improvement. 164(4): 213-224.

Ngo, T. and Indraratna, B., (2020). Mitigating ballast degradation with under-sleeper rubber pads: Experimental and numerical perspectives. *Computers and Geotechnics*, *122*, p.103540.

Zhou, Y.G., Liu, K., Sun, Z.B. and Chen, Y.M., 2021. Liquefaction mitigation mechanisms of stone column-improved ground by dynamic centrifuge model tests. Soil Dynamics and Earthquake Engineering, 150, p.106946.

Siahaan, F., Kelly, and Wong. (2011). "*Performance of an embankment constructed on stone columns*". International Conference on Advances in Geotechnical Engineering, Australia.

Sivakumar, V., Jeludine, D. K. N. M., Bell, A., Glynn, D. T. , and Mackinnon, P. (2011). "*The pressure distribution along stone columns in soft clay under consolidation and foundation loading*". Géotechnique. 61(7): 613-620.

Song, W., Huang, Stránský J., and Wu H., 2019. *Interaction between Railroad Ballast and Sleeper: A DEM-FEM Approach.* International Journal of Geomechanics, **19**(5): p. 04019030.